G. Ablations

We extend the results from the main paper by running multiple ablation studies mainly focusing on (a) the individual and combined impact of SPH relaxation and force treatment on the example of **dam break**, (b) the sensitivity of the parameters governing the proposed SPH relaxation on the example of **lid-driven cavity**, and (c) the impact of smoothing the external force function on the example of the **reverse Poiseuille flow** datasets. We believe that this exhaustive analysis of the hyperparameters is essential for practitioners who would consider using our proposed methods. To increase the value of the analysis we add (A) the evolution of the metrics over the simulation length, (B) error bars representing the 0.25 and 0.75 quantiles over the test trajectories, and (C) three more metrics compared to the main paper. The six metrics we use are:

1. MSE_{400} – position MSE over 400 steps.
2. MSE_{Ekin} – kinetic energy MSE between the predicted and ground truth frames.
3. Sinkhorn – Sinkhorn divergence between the particle distribution of predicted and ground truth frames.
4. MAE_{ρ} – density MAE error measuring the deviation of the density from the reference density ρ_{ref}. In all our experiments $\rho_{ref} = 1.0$.
5. Dirichlet – Dirichlet energy of density field as defined in Eq. 7.
6. Chamfer – symmetric Chamfer distance between predicted and ground truth frames.

G.1. Dam Break

We compare the impact of our external force treatment ($\square_g$), our SPH relaxation with parameters from Table 2 ($\square_p$), and combination of both ($\square_{g,p}$) on the dam break dataset using the GNS (Fig. 11) and SEGNN (Fig. 12). On the MSE_{Ekin} we see that only through the combination of our force treatment and SPH relaxation we achieve significant performance boosts with both the GNS and SEGNN models.

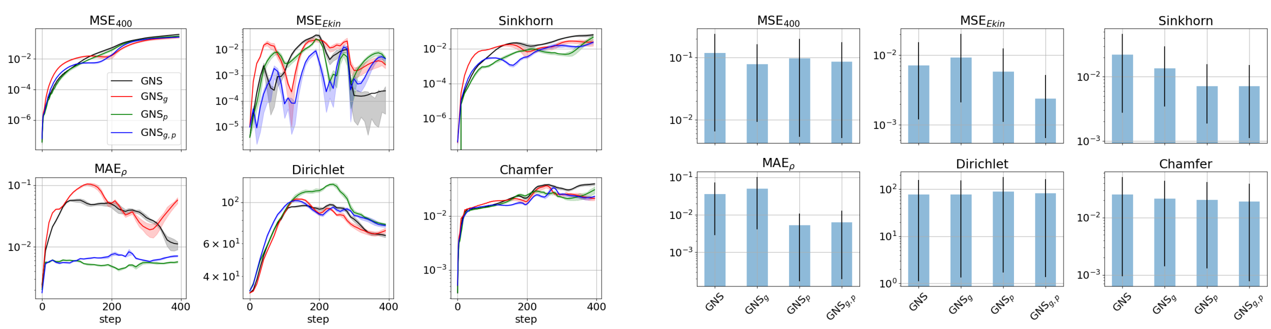

Figure 11. Ablations on DAM 2D with GNS-10-128 over the simulation length (left) and the average thereof (right).

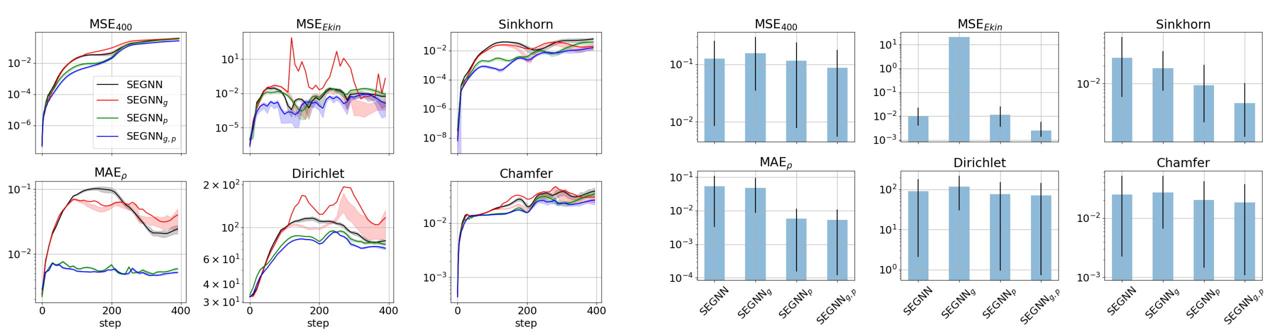

Figure 12. Ablations on DAM 2D with SEGNN-10-64 over the simulation length (left) and the average thereof (right).

G.2. Lid-Driven Cavity

We investigate the influence of the relaxation hyperparameters α and β from Eq. 5 and the number of relaxation steps/loops. The evolution of the six error measures over the 400 steps is shown on the left, and the average for each hyperparameter configuration is shown on the right. Intervals indicate the 0.25 and 0.75 quantiles over the 12 test trajectories (left) and the average of those values over the 400 steps (right).

G.2.1. LDC 2D WITH GNS

Based on Fig. 13, we choose $\alpha = 0.03$ as beyond this value, the Dirichlet energy starts increasing, indicating instabilities. In Fig. 14, we see on MSE_{400} and MSE_{Ekin} that beyond 5 iterations the accuracy drops, so we choose $l = 5$ loops. In Fig. 15, we don't see performance gains using the viscous term, so we decide not to use it.

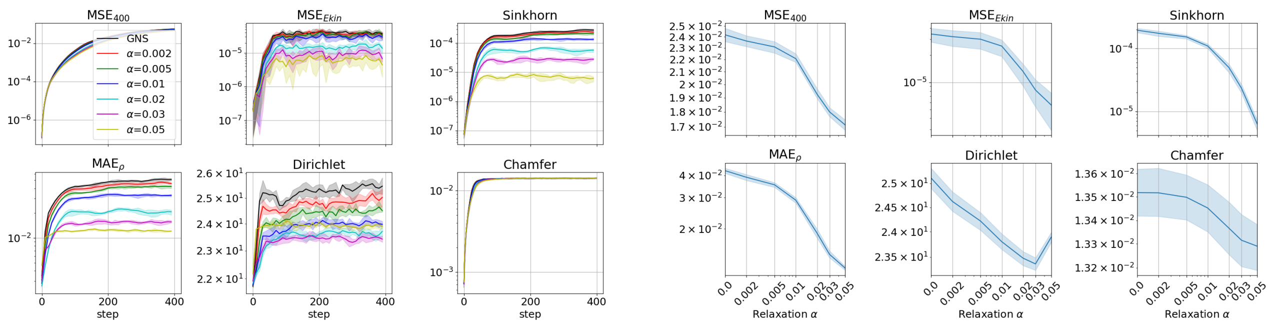

Figure 13. Ablations on LDC 2D with GNS-10-128 ($l = 1$) regarding relaxation parameter α.

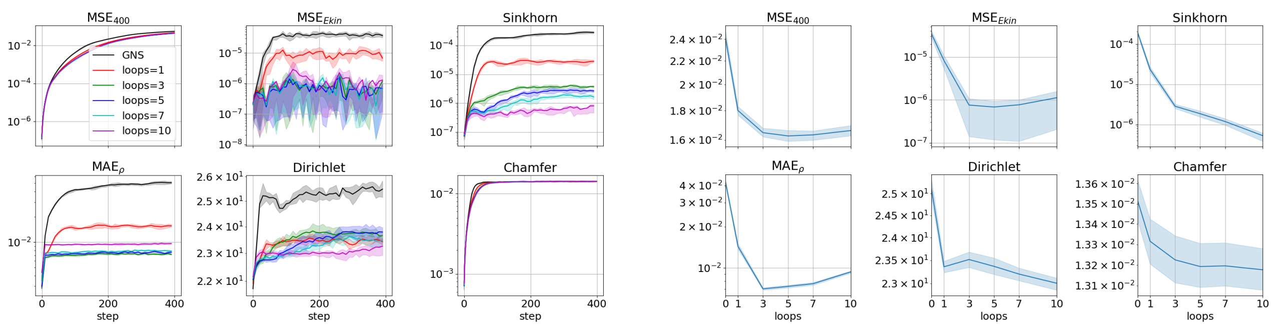

Figure 14. Ablations on LDC 2D with GNS-10-128 ($\alpha = 0.03$) regarding the number of relaxation steps/loops.

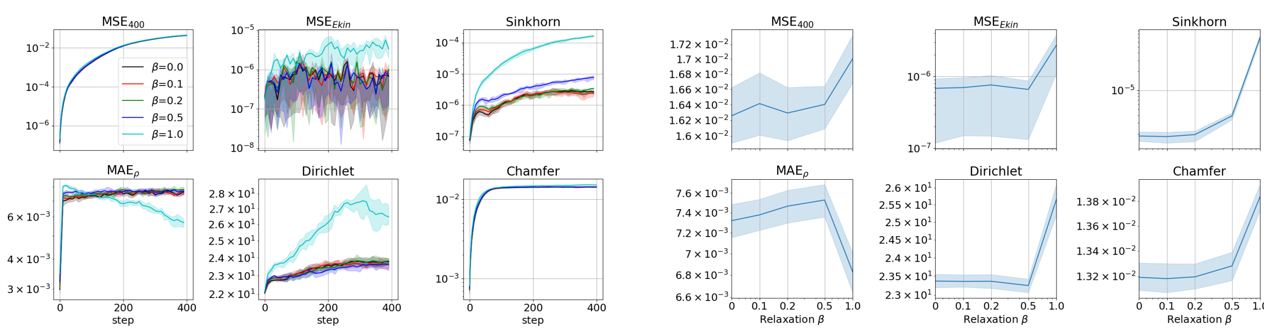

Figure 15. Ablations on LDC 2D with GNS-10-128 ($\alpha = 0.03$, $l = 5$) regarding relaxation parameter β.

G.2.2. LDC 2D WITH SEGNN

We again stress that the relaxation hyperparameters were optimized on GNS and we only ablate their influence on the performance of SEGNN. But we indeed observe similar behavior between GNS and SEGNN. We do stress the dramatic improvement in performance upon 5 and more relaxation steps visible in Fig. 17. In contrast to GNS, we do see positive impact of the viscous term on SEGNN, and would recommend using $\beta = 0.5$, see Fig. 18.

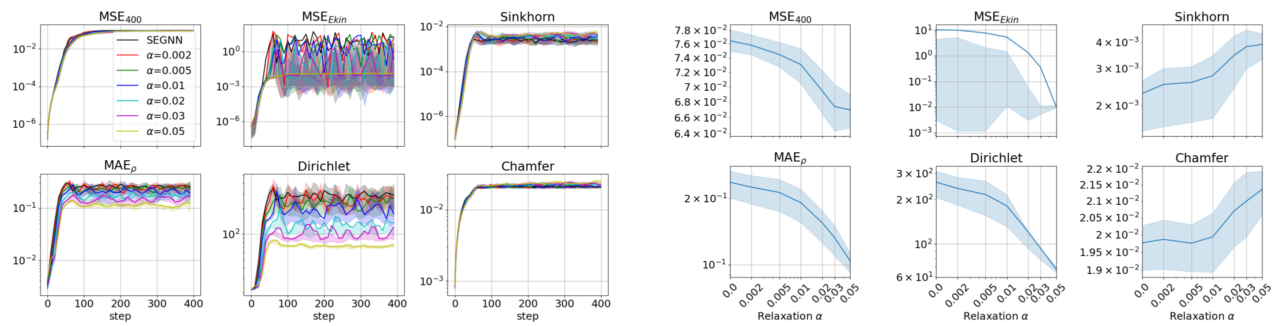

Figure 16. Ablations on LDC 2D with SEGNN-10-64 ($l = 1$) regarding relaxation parameter α.

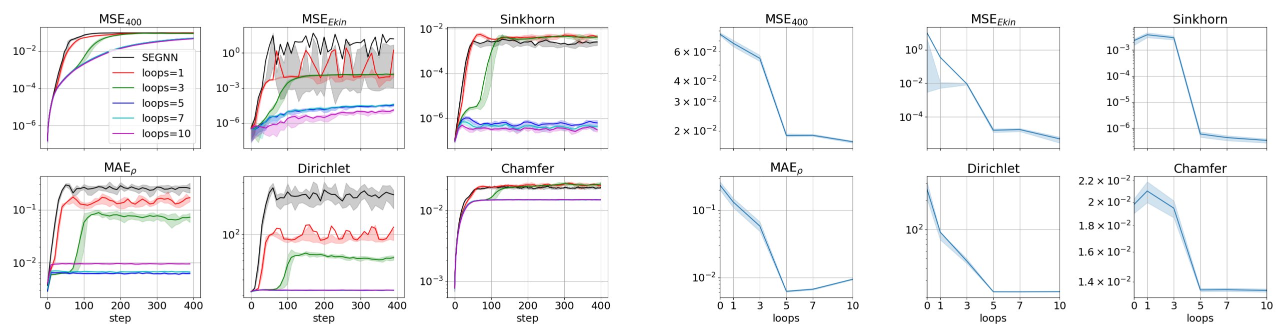

Figure 17. Ablations on LDC 2D with SEGNN-10-64 ($\alpha = 0.03$) regarding the number of relaxation steps/loops.

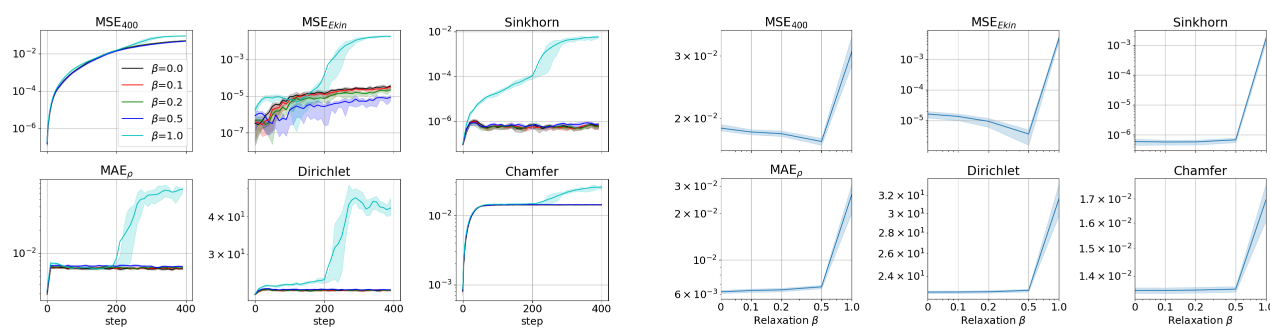

Figure 18. Ablations on LDC 2D with SEGNN-10-64 ($\alpha = 0.03$, $l = 5$) regarding relaxation parameter β.

G.2.3. LDC 3D WITH GNS

These plots agree with our choice of hyperparameters from Table 2 and show the sensitivity with respect to the relaxation parameters.

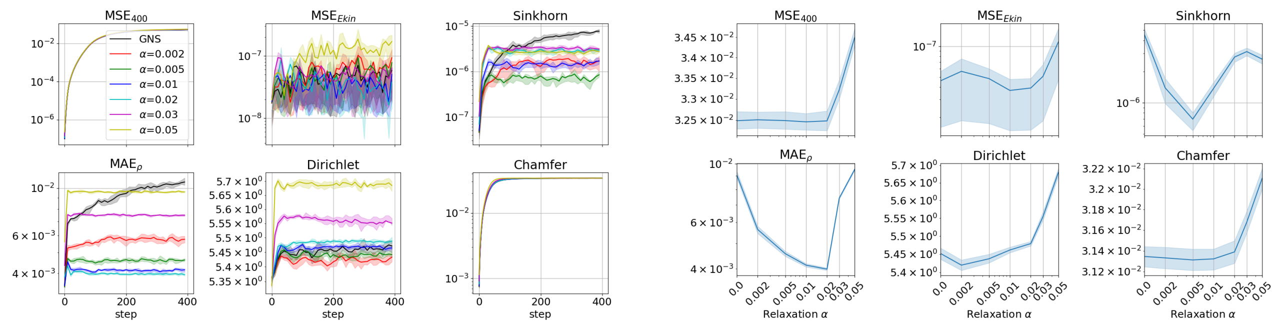

Figure 19. Ablations on LDC 3D with GNS-10-128 ($l = 1$) regarding relaxation parameter α.

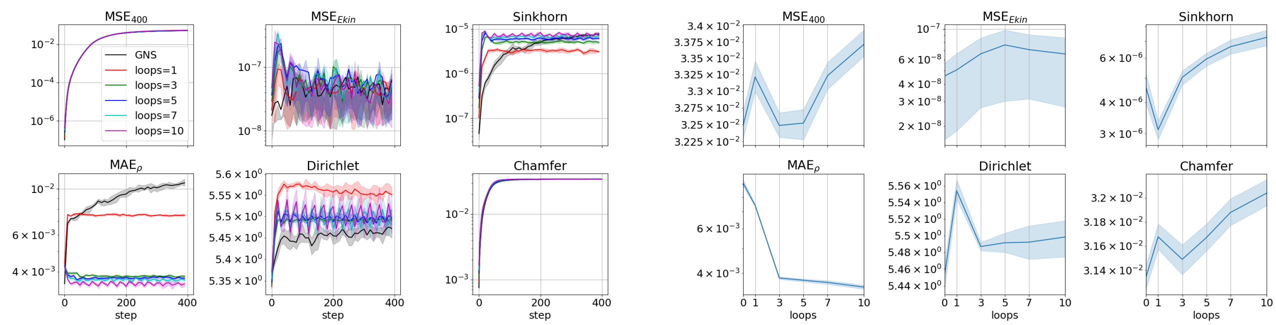

Figure 20. Ablations on LDC 3D with GNS-10-128 ($\alpha = 0.02$) regarding the number of relaxation steps/loops.

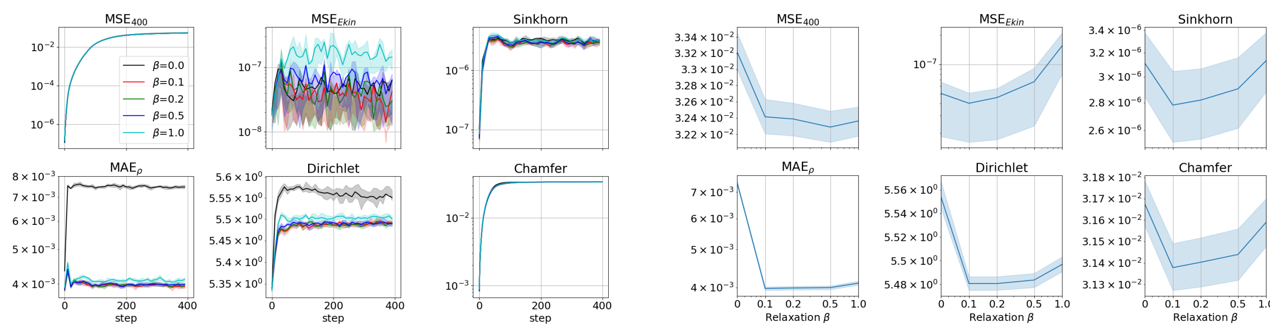

Figure 21. Ablations on LDC 3D with GNS-10-128 ($\alpha = 0.02$, $l = 1$) regarding relaxation parameter β.

G.2.4. LDC 3D WITH SEGNN

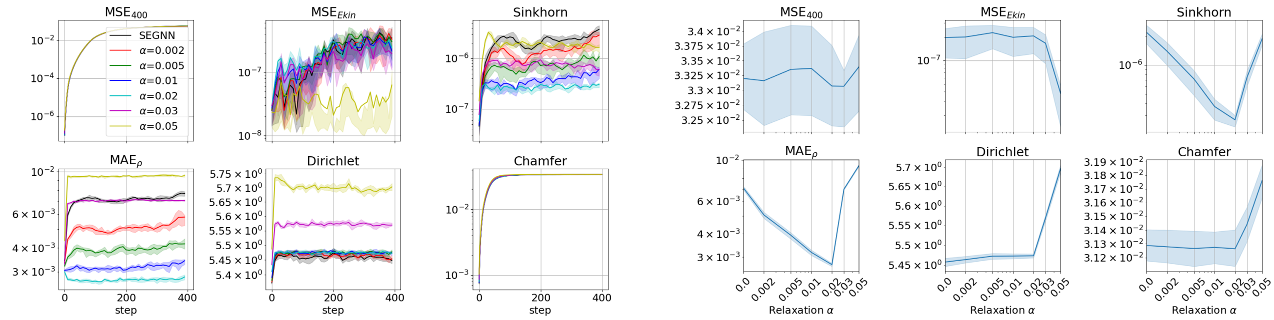

Figure 22. Ablations on LDC 3D with SEGNN-10-64 ($l = 1$) regarding relaxation parameter α.

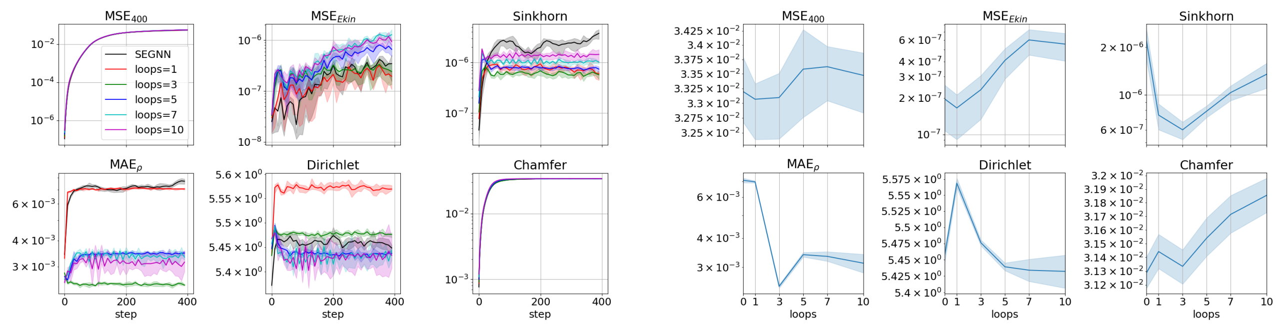

Figure 23. Ablations on LDC 3D with SEGNN-10-64 ($\alpha = 0.02$) regarding the number of relaxation steps/loops.

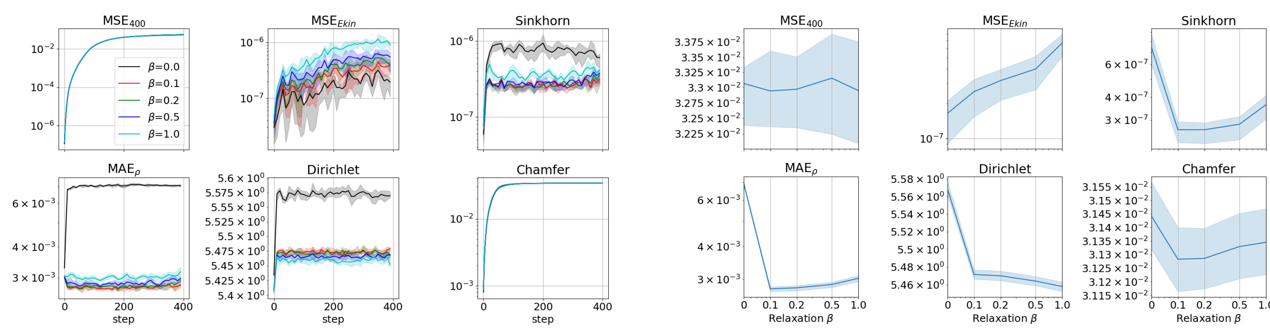

Figure 24. Ablations on LDC 3D with SEGNN-10-64 ($\alpha = 0.02$, $l = 1$) regarding relaxation parameter β.

G.3. Reverse Poiseuille Flow

We compare all variants of RPF model from the main paper with the case of not smoothing the external force, denoted $\square_{g_{raw}}$. The main message with regard to excluding the external force from the training target (all methods with $\square_g$) is that not smoothing the force function when the it has discontinuities leads to a highly unstable models, see MSE$_{Ekin}$ in Figs. 26, 27. It is probably a matter of too few test trajectories that we don't observe such blow ups in Figs. 25, 28.

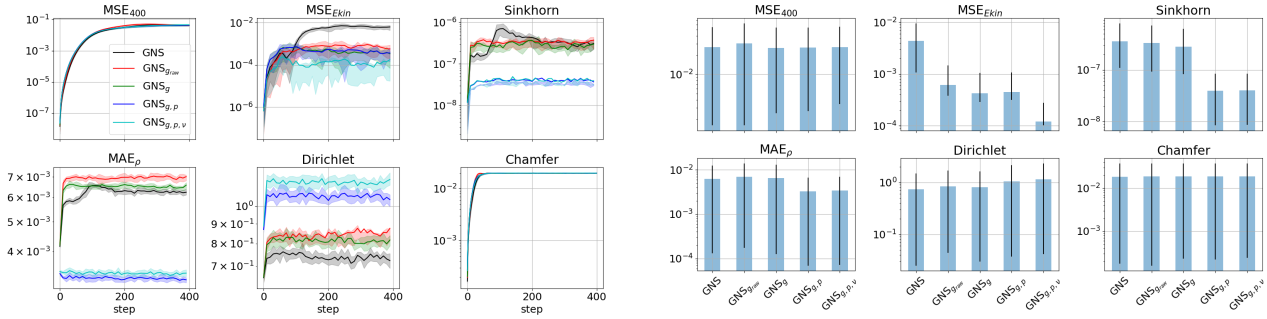

Figure 25. Ablations on RPF 2D with GNS-10-128 over the simulation length (left) and the average thereof (right).

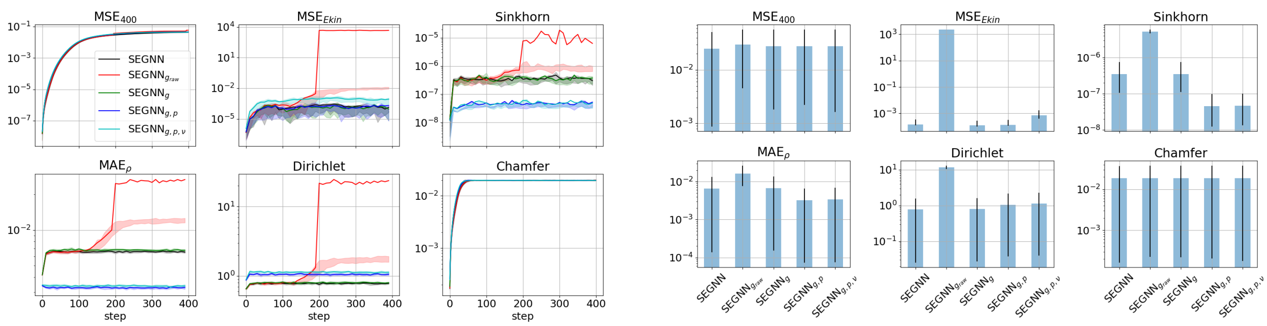

Figure 26. Ablations on RPF 2D with SEGNN-10-64 over the simulation length (left) and the average thereof (right).

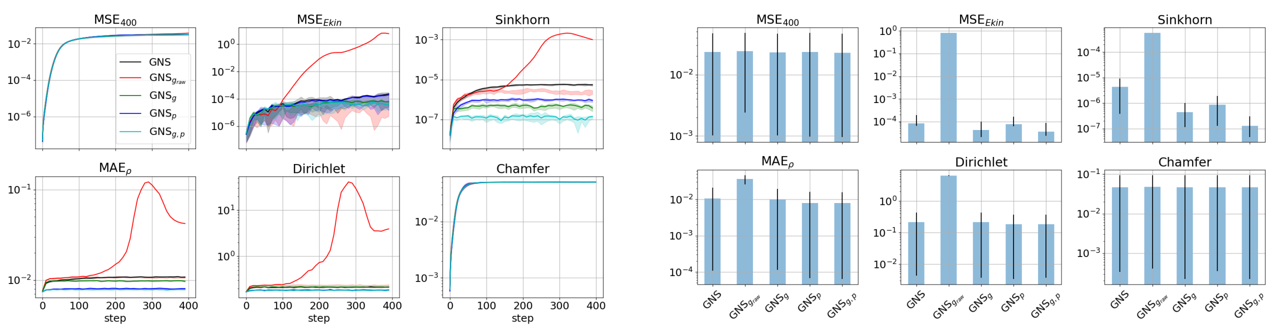

Figure 27. Ablations on RPF 3D with GNS-10-128 over the simulation length (left) and the average thereof (right).

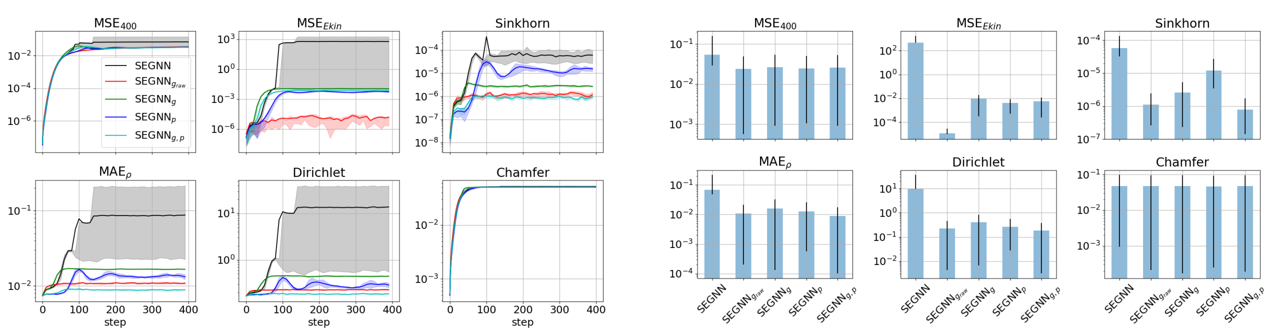

Figure 28. Ablations on RPF 3D with SEGNN-10-64 over the simulation length (left) and the average thereof (right).